Accepted Manuscript

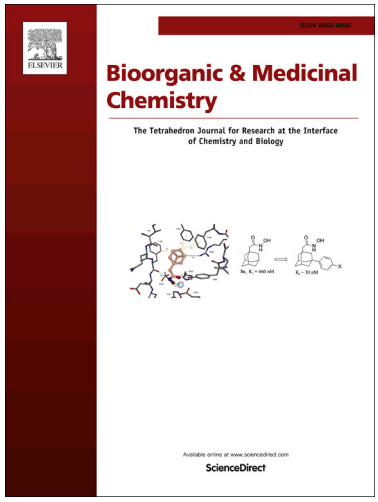

Benzoic acid derivatives with improved antifungal activity: design, synthesis, structure–activity relationship (SAR) and CYP53 docking studies

Sabina Berne, Lidija Kovačič, Matej Sova, Nada Kraševec, Stanislav Gobec, Igor Križaj, Radovan Komel

PII: S0968-0896(15)00536-2
DOI: http://dx.doi.org/10.1016/j.bmc.2015.06.042
Reference: BMC 12398

To appear in: *Bioorganic & Medicinal Chemistry*

Received Date: 20 February 2015
Revised Date: 15 June 2015
Accepted Date: 16 June 2015

Please cite this article as: Berne, S., Kovačič, L., Sova, M., Kraševec, N., Gobec, S., Križaj, I., Komel, R., Benzoic acid derivatives with improved antifungal activity: design, synthesis, structure–activity relationship (SAR) and CYP53 docking studies, *Bioorganic & Medicinal Chemistry* (2015), doi: http://dx.doi.org/10.1016/j.bmc.2015.06.042

Graphical Abstract

Benzoic acid derivatives with improved antifungal activity: design, synthesis, structure–activity relationship (SAR) and CYP53 docking studies

Leave this area blank for abstract info.

Sabina Berne[a,*], Lidija Kovačič[b,c], Matej Sova[d], Nada Kraševec[e], Stanislav Gobec[d], Igor Križaj[b,f] and Radovan Komel[a,e,*]

[a]*Institute of Biochemistry, Faculty of Medicine, University of Ljubljana, Vrazov trg 2, SI-1000 Ljubljana, Slovenia*

[b]*Department of Molecular and Biomedical Sciences, Jožef Stefan Institute, Jamova 39, SI-1000 Ljubljana, Slovenia*

[c]*UCD Conway Institute, School of Medicine and Medical Science, University College Dublin, Belfield, Dublin 4, Ireland*

[d]*Chair of Pharmaceutical Chemistry, Faculty of Pharmacy, University of Ljubljana, Aškerčeva cesta 7, SI-1000 Ljubljana, Slovenia*

[e]*National Institute of Chemistry, Hajdrihova 19, SI-1000 Ljubljana, Slovenia*

[f]*Department of Chemistry and Biochemistry, Faculty of Chemistry and Chemical Technology, University of Ljubljana, Večna pot 113, SI-1000 Ljubljana, Slovenia*

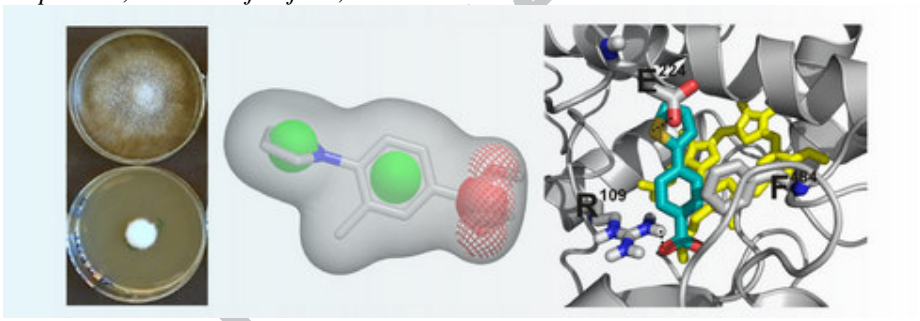

Bioorganic & Medicinal Chemistry
journal homepage: www.elsevier.com

Benzoic acid derivatives with improved antifungal activity: design, synthesis, structure–activity relationship (SAR) and CYP53 docking studies

Sabina Berne[a,*], Lidija Kovačič[b,c], Matej Sova[d], Nada Kraševec[e], **Stanislav Gobec**[d], **Igor Križaj**[b,f] and Radovan Komel[a,e,*]

[a]*Institute of Biochemistry, Faculty of Medicine, University of Ljubljana, Vrazov trg 2, SI-1000 Ljubljana, Slovenia*
[b]*Department of Molecular and Biomedical Sciences, Jožef Stefan Institute, Jamova 39, SI-1000 Ljubljana, Slovenia*
[c]*UCD Conway Institute, School of Medicine and Medical Science, University College Dublin, Belfield, Dublin 4, Ireland*
[d]*Chair of Pharmaceutical Chemistry, Faculty of Pharmacy, University of Ljubljana, Aškerčeva cesta 7, SI-1000 Ljubljana, Slovenia*
[e]*National Institute of Chemistry, Hajdrihova 19, SI-1000 Ljubljana, Slovenia*
[f]*Department of Chemistry and Biochemistry, Faculty of Chemistry and Chemical Technology, University of Ljubljana, Večna pot 113, SI-1000 Ljubljana, Slovenia*

ARTICLE INFO

Article history:
Received
Received in revised form
Accepted
Available online

Keywords:
Benzoic acid;
CYP53;
Cytochrome P450;
SAR;
Molecular modeling;
Molecular docking;
Antifungal activity.

ABSTRACT

Previously, we identified CYP53 as a fungal-specific target of natural phenolic antifungal compounds and discovered several inhibitors with antifungal properties. In this study, we performed similarity-based virtual screening and synthesis to obtain benzoic acid-derived compounds and assessed their antifungal activity against *Cochliobolus lunatus*, *Aspergillus niger* and *Pleurotus ostreatus*. In addition, we generated structural models of CYP53 enzyme and used them in docking trials with 40 selected compounds. Finally, we explored CYP53-ligand interactions and identified structural elements conferring increased antifungal activity to facilitate the development of potential new antifungal agents that specifically target CYP53 enzymes of animal and plant pathogenic fungi.

1. Introduction

Fungal diseases are not only becoming an increasing economic burden in healthcare [1] and jeopardizing food security [2] but also pose a threat to plant and animal biodiversity [3]. Despite the high demand for antifungal compounds with novel chemical scaffolds and modes of action, the development of antifungal agents is relatively slow.[4] Due to the eukaryotic nature of fungal cells, it is difficult to find appropriate fungal-specific targets.[5] Furthermore, structure-based drug design is limited by the scarce availability of three-dimensional (3D) structures of known fungal drug targets.[4] Nevertheless, significant technological advances have been made to accelerate antifungal drug discovery. Genome information from over 350 fungal species [6] enables the identification of new molecular targets by comparative genomics tools [7]. Modern computer-aided drug design approaches [8] combined with new high-throughput screening assays [9,10] against natural products and chemical libraries provide rapid selection and evaluation of potential antifungal drug candidates.

Numerous and highly diverse cytochromes P450 (CYPs) have been found in fungal genomes.[11] Apart from their roles in the primary and secondary metabolism, certain fungal CYPs are targets of antifungal drugs and agrochemicals (e.g., CYP51).[12] We previously established that benzoate 4-monooxygenase (CYP53A15) from the plant pathogenic Dothidiomycete *Cochliobolus lunatus* (*Curvularia lunata*) is a target of natural phenolic antifungal compounds and proposed CYP53 family members as potential novel antifungal targets.[13] The CYP53 family is fairly conserved and widely distributed among ascomycete and basidiomycete fungi but so far unidentified in ascomycete yeasts.[14] Initially, fungal CYP53 family members were characterized as detoxifying enzymes that convert benzoate and certain mono-substituted benzoate derivatives to 4-

* Corresponding author. Tel.: +386-1-320-3296; fax: +386-1-423-1088; e-mail: sabina.berne@mf.uni-lj.si or sabina.berne@bf.uni-lj.si

Present address: Department of Agronomy, Biotechnical Faculty, Jamnikarjeva 101, SI-1000 Ljubljana, Slovenia.

* Corresponding author. Tel.: +386-1-543-7662; fax: +386-1-543-7641; e-mail: radovan.komel@mf.uni-lj.si

hydroxylated products.[15–18] These are further metabolized via the β-ketoadipate pathway for aromatic compound degradation to produce intermediates that finally enter the tricarboxylic acid cycle and are utilized as a source of carbon.[19] However, some CYP53 members also exhibit O-demethylation activity of 3-methoxybenzoate derivatives.[13,16] Recently, a peculiar O-demethylation of stilbene derivatives has been demonstrated for CYP53D2 from *Postia placenta*.[20] In addition to a proposed biological role of CYP53 in the degradation of plant-based aromatic compounds (e.g., released in soil or dead plant material) [21], it is possible that benzoate detoxification in plant pathogenic fungi contributes to their pathogenicity. Indeed, during infection of maize, up-regulated expression of benzoate 4-monooxygenase gene (*BPH*) from the pathogenic Dothideomycete fungus *Cochliobolus heterostrophus* (*Bipolaris maydis*) has been reported.[22]

Building on these findings, we have already identified new antifungal compounds that specifically inhibit the catalytic activity of CYP53A15 and restrain mycelial growth of *Cochliobolus lunatus*, *Aspergillus niger* and *Pleurotus ostreatus*.[23,24] Since benzoic and cinnamic acid derivatives tested against these fungi displayed only moderate antifungal activity the present study focuses primarily on the structure-antifungal activity analyses to determine key structural features of the inhibitors that bestow increased antifungal effects. Exploration of the nature of CYP53-ligand interactions was performed by HADDOCK[25] that requires prior knowledge of biochemical and biophysical interaction data and to these end the results obtained from our previous studies[23,24] served as a good basis. By homology modeling we first generated structural models of three fungal CYP53 enzymes: i) CYP53A1 from *Aspergillus niger*, the first fungal benzoate para-hydroxylase to be purified and biochemically characterized, ii) CYP53A15 from *Cochliobolus lunatus*, also well characterized protein and an object of our research for the past decade and iii) CYP53C11 from *Pleurotus ostreatus* selected due to higher identity to CYP53A15 (54%) and CYP53A1 (50%) in comparison to the other two predicted CYP53 sequences in its genome. We then carried out ligand-based virtual screening with best hit compound[23] **1a** as a template and obtained 40 compounds that were screened for antifungal activity against these fungal species. We finally correlated antifungal activity with compounds' structural features and investigated CYP53 enzyme-ligand interactions by docking experiments using HADDOCK. The structural insights into individual/common characteristics of the CYP53 active sites and enzyme-inhibitor interactions will contribute to the design and development of potential new antifungal compounds.

2. Materials and methods

2.1. Compound selection using ligand-based virtual screening

For the ligand-based virtual screening, we selected the "drug-like" subset of the ZINC database [26], with 13 million compounds, and downloaded it in SD format. We first prepared the database with Omega 2.4 software (OpenEye Scientific Software, Santa Fe, NM. http://www.eyesopen.com) to yield an average of 152 conformations per compound. We then screened this database using ROCS 3 software (OpenEye Scientific Software, Santa Fe, NM. http://www.eyesopen.com) to reduce it to compounds that fit well to the query compound in terms of size and shape (Figure 1), **3-methyl-4-(1H-pyrrol-1-yl)benzoic acid** (**1a**; the best compound from the first round of virtual screening [23]).

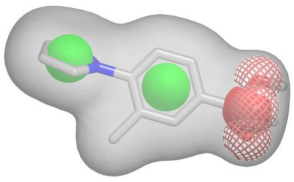

Figure 1. The shape and atom types of query compound **1a** used for similarity-based virtual screening. The compound shape is presented in grey, atom types are colored: ring systems (green), anions (red), H-bond acceptors (red net).

2.2. Compound characterization

Compound **1a** was obtained from ChemBridge (http://www.chembridge.com), compounds **14** and **17** from Maybridge (http://www.maybridge.com), compounds **11**, **12**, **28** and **33** from Vitas-M Laboratories (http://www.vitasmlab.com), compounds **13**, **19**, **21**, **22**, **23** and **29** from Key Organics (http://www.keyorganics.net), compounds **3**, **8**, **16**, **18** and **32** from Specs (http://www.specs.net), compounds **4**, **7** and **10** from Mir Biotech (http://www.mirbiotech.com), compounds **5**, **6** and **20** from Princeton BioMolecular Research (http://www.princetonbio.com), compounds **15, 24**, **25**, **26** and **30** from Combi-Block (http://www.combi-blocks.com), compound **31** from UkrOrgSynthesis (http://www.ukrorgsynth.com), compounds **34** and **36** from Fluka (http://www.sigmaaldrich.com) and compounds **36** and **35** from Acros Organics (http://www.acros.com). The reagents and solvents for chemical synthesis were purchased from Acros Organics, Sigma-Aldrich and Maybridge and used without further purification. Analytical TLC was performed on Merck silica gel ($60F_{254}$) pre-coated plates (0.25 mm) and the compounds were visualized under UV light. Column chromatography was carried out on the Merck silica gel 60 (mesh 70-230). The yields of purified products were not optimized. The compounds' melting points were determined on a Reichert hot-stage apparatus and are presented as uncorrected values. The molecular formulas of the compounds were identified and confirmed by mass spectral data and high-resolution mass measurements on a VG-Analytical Autospec Q mass spectrometer. IR spectra were recorded on a Perkin-Elmer FTIR 1600 spectrometer.

2.2.1. NMR spectra.

^{1}H and ^{13}C NMR spectra were recorded on a Bruker Avance 400 DPX spectrometer at 298 K. The values are reported in ppm using tetramethylsilane or solvent as internal standard (DMSO-d_6 at 2.50 ppm, $CDCl_3$ at 7.26 ppm). The coupling constants (J) are in Hz and the splitting patterns are designated: s, singlet; br s, broad singlet; d, doublet; dd, double doublet; ddd, doublet of doublet of doublet; t, triplet; dt, double triplet; and m, multiplet.

2.2.2. HPLC analysis.

The purities of all active compounds were determined by reversed-phase high-performance liquid chromatography (HPLC) analysis on an Agilent 1100 system (Agilent Technologies, Santa Clara, CA, USA) equipped with a quaternary pump and a multiple-wavelength detector, using an Agilent Eclipse Plus C18, 5 µm column (4.6 × 50 mm, 5 µm), with a flow rate of 1.0 mL/min, detection at 254 nm and an eluent system of: A = 0.1% TFA in H_2O; B = MeOH. The following gradient was applied:

i) method 1: 0–16 min, 10% B → 90% B in A; 16–19 min, 90% B in A; 19–20 min, 90% B → 10% B in A; post time 6 min. The run time was 26 min, at a temperature of 25 °C;

ii) method 2: 0–12 min, 50% B → 90% B in A; 12–16 min, 90% B in A; 16-20 min, 90% B → 50% B in A; post time 6 min. The run time was 26 min, at a temperature of 25 °C.

The relative purity of all active compounds was above 95.0% as determined by HPLC.

*2.3. Synthesis of compounds **1b**, **2**, **9** and **27**.*

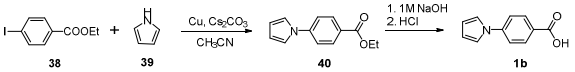

Scheme 1. Synthesis of compound **1b**.

Ethyl 4-(1H-pyrrol-1-yl)benzoate (**40**): Compound **40** was synthesized according to the published procedure [27]. Cesium carbonate (978 mg, 12.0 mmol), copper (75 mg, 1.2 mmol) and anhydrous acetonitrile (24 ml) were added to a dry flask (equipped with a magnetic stirrer and a rubber septum) filled with argon. Ethyl 4-iodobenzoate **38** (1.0 ml, 6.0 mmol) and pyrrole **39** (0.7 mM, 9.0 mmol) were added to the obtained suspension and stirred under reflux for 72 hours. Since TLC analysis of the reaction mixture showed an incomplete reaction, cesium carbonate (978 mg, 12.0 mmol) and copper (75 mg, 1.2 mmol) were added again and the reaction mixture was stirred under reflux for an additional 48 hours and then cooled to room temperature. The solid was filtered off and washed with ethylacetate. The combined organic phases were removed by evaporation and the obtained residue was purified by column chromatography using diethylether/hexane (1/10) as an eluent to obtain 0.581 g (45%) of compound **40** as white crystals. Mp 78-79°C; ^{1}H-NMR (400 MHz, $CDCl_3$) δ(ppm): 1.32 (t, *J* = 7.2 Hz, 3H, CH_3), 4.30 (q, *J* = 7.2 Hz, 2H, CH_2), 6.29 (t, *J* = 2.2 Hz, 2H, pyrrole-H), 7.07 (t, *J* = 2.2 Hz, 2H, pyrrole-H), 7.35 (d, *J* = 8.8 Hz, 2H, Ar-H), 8.01 (d, *J* = 8.8 Hz, 2H, Ar-H); HR-MS (ESI): *m/z* calcd. for C13H14NO2 $[M+H]^+$ 216.1025, found: 216.1025.

4-(1H-pyrrol-1-yl)benzoic acid (**1b**): Compound **40** (490 mg, 1.75 mmol) was suspended in 10 ml of 1 M NaOH and stirred at room temperature for 48 hours; 1 M HCl was then added dropwise to adjust the pH to 1 and the white solid was filtered off and dried to obtain 0.083 g (19%) of compound **1b** as a light brown solid. Mp 198-202°C; ^{1}H-NMR (400 MHz, DMSO-*d*6) δ(ppm): 6.32 (t, *J* = 2.4 Hz, 2H, pyrrole-H), 7.50 (t, *J* = 2.2 Hz, 2H, pyrrole-H), 7.70-7.74 (m, 2H, Ar-H), 7.98-8.01 (m, *J* = 8.8 Hz, 2H, Ar-H); 1H from COOH is exchanged; ^{13}C-NMR (100 MHz, DMSO-*d*6: δ(ppm) 111.4, 118.6, 119.1, 127.1, 131.0, 143.0, 166.0; HR-MS (ESI): *m/z* calcd. for C11H10NO2 $[M+H]^+$ 188.0712, found: 188.0716; HPLC t_R = 16.054 min (95.4%, Method 1).

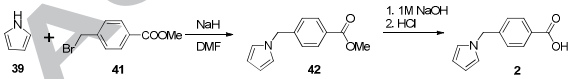

Scheme 2. Synthesis of compound **2**.

Methyl 4-(pyrrol-1-ylmethyl)benzoate (**42**). Pyrrole **39** (0.201 g, 3.0 mmol) and NaH (108 mg, 4.5 mmol) were dissolved in anhydrous DMF (10 mL) and the mixture was cooled to 0ºC under an argon atmosphere. After 30 minutes, methyl 4-(bromomethyl)benzoate **41** (0.756 g; 3.3 mmol) was added, the ice bath was removed and the mixture was stirred for 72 hours at 55°C. The reaction mixture was then cooled to room temperature and 30 ml of saturated $NaHCO_3$ were slowly added. The obtained solution was washed with ethylacetate (50 mL). After layer separation, the organic phase was dried with anhydrous Na_2SO_4, filtered and the solvent was removed by evaporation. The residue was purified by column chromatography using ethylacetate/hexane (1/6 to 1/4) as an eluent to obtain compound **42** as white needle crystals. Yield 44 %; mp 27-28°C; ^{1}H-NMR (400 MHz, $CDCl_3$): δ(ppm) 3.93 (s, 3H, CH_3), 5.16 (s, 2H, CH_2), 6.24 (t, *J*= 2.0 Hz, 2H, Ar-H), 6.72 (t, *J*= 2.0 Hz, 2H, Ar-H), 7.17 (d, *J*= 8.0 Hz, 2H, Ar-H); 8.01 (d, *J*= 8.0 Hz, 2H, Ar-H); HR-MS (ESI): *m/z* calcd. for C13H14NO2 $[M+H]^+$ 216.1025, found: 216.1029; HPLC t_R = 9.832 min (Method 2). The data are consistent with those reported previously.[28]

4-(pyrrol-1-ylmethyl)benzoic acid (**2**). Methyl 4-(pyrrol-1-ylmethyl)benzoate (**42**) (196 mg, 0.91 mmol) was suspended in 1 M NaOH (10.0 mL, 10.0 mmol) and stirred at room temperature for 24 hours; 2.0 ml of dioxane were then added and stirred at room temperature for an additional 72 hours. The pH was adjusted to 1 by the addition of 1 M HCl and the white solid was filtered off to obtain compound **2** as white needles. Yield 94%; mp 152-155°C; ^{1}H-NMR (400 MHz, DMSO-*d*6): δ(ppm) 5.19 (s, CH_2), 6.04 (s, 2H, Ar-H), 6.82 (s, 2H, Ar-H), 7.23 (d, *J*= 7.6 Hz, 2H, Ar-H), 7.89 (d, *J*= 7.6Hz, 2H, Ar-H), 12.94 (br s, 1H, COOH); HR-MS (ESI): *m/z* calcd. for C12H10NO2 $[M-H]^-$ 200.0712, found: 200.0710; HPLC t_R = 7.616 min (Method 2).

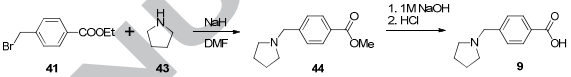

Scheme 3. Synthesis of compound **9**.

Methyl 4-(pyrrolidin-1-ylmethyl)benzoate (**44**). Pyrrolidine **43** (0.246 mL, 3.0 mmol) and NaH (108 mg, 4.5 mmol) were dissolved in anhydrous DMF (10 mL) and cooled to 0ºC under an argon atmosphere. After 30 minutes, methyl 4-(bromomethyl)benzoate **41** (0.756 g; 3.3 mmol) was added, the ice bath was removed and the mixture was stirred at room temperature for 24 hours; 30 ml of saturated $NaHCO_3$ were then slowly added and the obtained solution was washed with ethylacetate (50 mL). After layer separation, the organic phase was dried with anhydrous Na_2SO_4, filtered and the solvent was removed by evaporation. The oil residue was purified by column chromatography using methanol/ethylacetate (7/1) as an eluent to obtain compound **44** as a slightly yellow viscous liquid. Yield 52%; ^{1}H-NMR (400 MHz, $CDCl_3$): δ(ppm) 1.78-1.81 (m, 4H, 2x CH_2), 2.49-2.52 (s, 4H, 2xCH_2), 3.66 (s, 2H, CH_2-Ph), 3.91 (s, 3H, CH_3), 7.41 (d, *J*= 7.6 Hz, 2H, Ar-H), 7.99 (d, *J*= 7.6 Hz, 2H, Ar-H); HR-MS (ESI): *m/z* calcd. for C13H18NO2 $[M+H]^+$ 220.1338, found: 220.1333. The data are consistent with those reported previously.[29]

4-(pyrrolidin-1-ylmethyl)benzoic acid (**9**): Methyl 4-(pyrrolidin-1-ylmethyl)benzoate (**44**) (193 mg, 0.88 mmol) was suspended in 1 M NaOH (5.0 mL, 5.0 mmol) and stirred at room temperature for 72 hours. The alkaline solution was washed with ethylacetate (10 mL) and 1 M HCl was then added to adjust the pH to 6. The solvent was removed by evaporation and the residue was purified by column chromatography using methanol/ethylacetate (2/1) as an eluent to obtain compound **9** as a white powder. Yield 95%; mp 229-231°C; ^{1}H-NMR (400 MHz, D_2O): δ(ppm) 1.72-1.76 (m, 4H, 2xCH_2), 2.53-2.57 (s, 4H, 2xCH_2), 3.68 (s, 2H, CH_2), 7.39 (d, *J*= 7.6 Hz, 2H, Ar-H), 7.81 (d, *J*=7.6 Hz, 2H, Ar-H), H from COOH is exchanged; HR-MS (ESI): *m/z* calcd. for C12H14NO2 $[M-H]^-$ 204.1025, found: 204.1019.

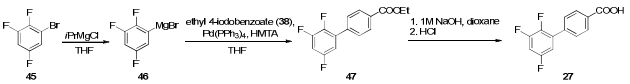

Scheme 4. Synthesis of compound **27**.

We synthesized compound **47** from Grignard reagent, prepared from 1-bromo-2,4,5-trifluorobenzene and ethyl 4-iodobenzoate (**38**).

Ethyl 2',4',5'-trifluoro-[1,1'-biphenyl]-4-carboxylate (**47**): To a dry flask (equipped with a magnetic stirrer and a rubber septum) filled with argon, 1-bromo-2,4,5-trifluorobenzene **45** (4.39 ml, 37.5 mol) and anhydrous THF (10.6 ml) were added and cooled to -20ºC; 2 M solution of iPrMgCl in THF (22.5 ml) was slowly added to the reaction mixture, the reaction temperature was adjusted to -10ºC and the mixture was stirred for one hour until the Grignard exchange reaction was completed. The resulting solution of **46** was added dropwise to the solution of ethyl 4-iodobenzoate **38** (0.50 ml, 3.0 mmol), tetrakis(triphenylphosphine)palladium (299 mg, 0.15 mmol) and HMTA (21 mg, 0.15 mmol) in anhydrous THF (20 ml) at 0ºC. The reaction mixture was maintained at 0ºC for one hour and then stirred overnight at room temperature. The solvent was removed by evaporation and the residue was purified by column chromatography using diethylether/hexane (1/10) as an eluent to obtain 0.70 g (83%) of compound **47** as white crystals. Mp 73-75°C; ^{1}H-NMR (400 MHz, $CDCl_3$): δ(ppm) 1.42 (t, J = 7.2 Hz, 3H, CH_3), 4.41 (q, J = 7.2 Hz, 2H, CH_2), 7.02-7.08 (m, 1H, Ar-H), 7.25-7.32 (m, 1H, Ar-H), 7.56 (d, J = 8.8 Hz, 2H, Ar-H), 8.12 (d, J = 8.8 Hz, 2H, Ar-H); ^{13}C-NMR (100 MHz, DMSO-d_6): δ(ppm) 14.08, 60.88, 106.80 (dd, 1H, $^{2}J_{C,F}$ = 21.2 Hz, $^{2}J_{C,F}$' = 29.7 Hz), 118.51 (dd, 1H, $^{3}J_{C,F}$ = 4.2 Hz, $^{2}J_{C,F}$ = 19.9 Hz), 124.00 (ddd, $^{3}J_{C,F}$ = 4.5 Hz, $^{3}J_{C,F}$ = 5.7 Hz, $^{2}J_{C,F}$ = 15.7 Hz), 129.14 (d, 1H, $^{3}J_{C,F}$ = 3.2 Hz), 129.35, 129.54, 137.71, 146.53 (ddd, $^{4}J_{C,F}$ = 3.3 Hz, $^{2}J_{C,F}$ = 13.6 Hz, $^{1}J_{C,F}$ = 241,4 Hz), 149.08 (dt, $^{3}J_{C,F}$ = 13.2 Hz, $^{2}J_{C,F}$ = 13.6 Hz, $^{1}J_{C,F}$ = 248.5 Hz), 154.39 (ddd, $^{4}J_{C,F}$ = 1.2 Hz, $^{3}J_{C,F}$ = 9.8 Hz, $^{1}J_{C,F}$ = 245,1 Hz), 165.28; HR-MS (ESI): *m/z* calcd. for $C_{15}H_{12}O_2F_3$ $[M+H]^+$ 281.0789, found: 281.0787; HPLC t_R = 13.669 min (97.2%, Method 2).

2',4',5'-trifluoro-[1,1'-biphenyl]-4-carboxylic acid (**27**): Compound **47** (490 mg, 1.75 mmol) was suspended in 12 ml of 1 M NaOH and 5 ml of dioxane and stirred for 24 hours; 1 M HCl was added dropwise to adjust the pH to 1 and the white solid was then filtered off and dried to obtain 0.43 g (97%) of compound **27** as white needles. Mp >300°C; ^{1}H-NMR (400 MHz, DMSO-*d6*): δ(ppm) 7.68-7.83 (m, 4H, Ar-H), 8.04 (dt, J = 8.4, 2.0 Hz, 2H, Ar-H), 13.13 (s, 1H, COOH); ^{13}C-NMR (100 MHz, DMSO-d_6): δ(ppm) 106.84 (dd, 1H, $^{2}J_{C,F}$ = 21.3 Hz, $^{2}J_{C,F}$' = 29.5 Hz), 118.59 (dd, 1H, $^{3}J_{C,F}$ = 4.4 Hz, $^{2}J_{C,F}$ = 19.8 Hz), 124.22 (ddd, $^{3}J_{C,F}$ = 4.4 Hz, $^{3}J_{C,F}$ = 6.2 Hz, $^{2}J_{C,F}$= 15.4 Hz), 129.10 (d, 1H, $^{3}J_{C,F}$ = 3.4 Hz), 129.62, 130.55, 137.45, 146.42 (dd, $^{4}J_{C,F}$= 3.2 Hz, $^{2}J_{C,F}$ = 12.4 Hz, $^{1}J_{C,F}$ = 241,0 Hz), 149.07 (dt, $^{3}J_{C,F}$= 12.9 Hz, $^{2}J_{C,F}$ = 14.3 Hz, $^{1}J_{C,F}$ = 249.0 Hz), 154.42 (ddd, $^{4}J_{C,F}$ = 2.2 Hz, $^{3}J_{C,F}$ = 9.8 Hz, $^{1}J_{C,F}$ = 245,9 Hz), 166.96; HR-MS (ESI): *m/z* calcd. for $C_{13}H_8O_2F_3$ $[M+H]^+$ 253.0476, found: 253.0477; HPLC t_R = 18.250 min (100%, Method 1).

2.4. Antifungal screening

The antifungal activity of compounds against *Cochliobolus lunatus* (*Curvularia lunata*) strain MUCL 38696 (m118), *Aspergillus niger* N402 *cspA1* and *Pleurotus ostreatus* Plo5 (ZIM collection of the Biotechnical Faculty, University of Ljubljana, Slovenia) was examined with a fungal growth based assay [24]. MEA (Blakeslee's formula) agar plates supplemented with inhibitor (0.1 mM final concentration) or control solvent were centrally inoculated with mycelial discs taken from 5-day-old fungal culture and fungal growth at 28°C was monitored daily. The fungal growth kinetics was determined using two parameters: radial growth rate (RGR) and initial growth inhibition (IGI).[30] To compare growth inhibition between the different fungi, fungal growth was expressed as percentage of the matching solvent control. All compounds were tested in triplicate. The most active compounds (**15**, **20** and **27**) were assessed in 2-4 independent experiments.

The antifungal activity of compounds was assessed also against a deletion mutant (Δ*bph*) of CYP53A15 from *C. lunatus*, prepared as described in [13], to determine if observed antifungal effects can be ascribed solely to the CYP53A15 or compounds interact also with other molecular targets contributing to the antifungal activity.

2.5. Sequential and structural conservation of CYP53 linked to functional relevance

FASTA formatted protein sequences of *Cochliobolus lunatus* CYP53A15 (protein ID: 52559), *Aspergillus niger* CYP53A1 (protein ID: 162813) and *Pleurotus ostreatus* CYP53C11 (protein ID: 175456) were acquired from the Joint Genome Institute at the U.S. Department of Energy (DOE-JGI; http://genome.jgi.doe.gov/programs/fungi/index.jsf) and aligned with the T-Coffee program at the European Bioinformatics Institute (EMBL-EBI). The CYP modules tool in the Cytochrome P450 Engineering Database [31] was used to predict structurally conserved regions of CYP53. Functionally relevant amino acid residues and regions of CYP53 (Figure 3) were marked, based on information from [32,33].

2.6. Modeling of CYP53 and selected compounds

By comparative modeling of fungal benzoate 4-monooxygenases, based on the available template three-dimensional (3D) model of *Cochliobolus lunatus* (PMDB ID: PM0075149; http://www.biocomputing.it/PMDB/) [13], 3D models of the enzyme soluble parts of CYP53A15 (*Cochliobolus lunatus*), CYP53A1 (*Aspergillus niger*) and CYP53C11 (*Pleurotus ostreatus*) were generated. Homology modeling was performed with the default parameters in Modeller 9v4 (http://www.salilab.org/modeller/), using the "allHmodel" protocol to include hydrogen atoms and the "HETATM" protocol to include HEM.

After initial docking trials with some of the previously published compounds[13], the models have been optimized to better fit the experimental data. For that purpose, several structures of *Bacillus megaterium* BM3 cytochrome P450 (PDB IDs: 1YQP, 4HGF, 4HGG, 4HGH and 4KEW), sharing 34% identity with our published template CYP53A15, were aligned and used for optimization of models in Modeller. All three models were then compared to the only available crystal structure of fungal cytochromes P450, CYP51 from *Saccharomyces cerevisiae* (PDB ID: 4LXJ; 20% sequence identity to CYP53A15).

Additionally, we checked models' quality by online version of SWISS-MODEL Workspace[34]. All models were subjected to Local Model Quality Estimation (Anolea - atomic mean force potential, QMEAN6 - Composite scoring function for model quality estimation), Global Model Quality Estimation (DFire - All-atom distance-dependent statistical potential) and to Stereochemistry Check (Procheck). Results (in Supporting Information) indicated that on average 99.9 % of all atoms in models were within the limits.

The atomic coordinates of most of the compounds were downloaded from ZINC database [26]. When the atomic coordinates of the compounds were not available in the database,

they were constructed based on the homology of the compound with a known structure.

2.7. Docking compounds in the active site of CYP53 models

The HADDOCK modeling program [25] was used for docking selected compounds based on previously known biochemical data and predicted biophysical interaction [13,23]. Docking was performed using the web server version of HADDOCK with a Guru interface and with most of the parameters set to default. For the enzyme-compound docking trials, compound active residues were set to all and passive residues to determine automatically. The active residues of the enzyme were predicted based on the CYP53A15-compound **1a** model [23]. For the clCYP53A15 enzyme model, the active residues were 41, 68, 69, 80, 83, 199, 364, 451 and 452; for the anCYP53A1 enzyme model, the active residues were 112, 136, 137, 138, 150, 153, 262 and 452; and for the poCYP53C11 enzyme model, the active residues were 79, 84, 108, 109, 123, 240, 243, 492 and 493, while the passive residues were set to determine automatically. In order to gain the van der Waals, electrostatic and desolvation energies for each enzyme-compound model, HADDOCK automatically performed molecular dynamics before and after each docking trial by including water in the calculation.

3. Results and discussion

3.1. Compound selection using Rapid Overlay of Chemical Structures (ROCS)

From the "drug-like" subset of the ZINC database [26], with over 13 million compounds, we retained 70 compounds with the highest shape and chemical similarity to 3-methyl-4-(1H-pyrrol-1-yl)benzoic acid (**1a**; Figure 1). We experimentally evaluated the 40 compounds listed in Supporting Information (SI) Table S1. To guide the structure-antifungal activity relationship studies, this list contains 30 compounds from ROCS screening selected according to market availability and price, 7 additionally synthesized or purchased compounds, the query compound (**1a**), as well as CYP53 substrate (benzoic acid; **BA**) and product (4-hydroxybenzoic acid; **4-HBA**).

3.2. Structural features of benzoic acid derivatives conferring antifungal activity

3.2.1. Inhibition of Cochliobolus lunatus growth.

Among the 40 compounds (SI Table S1) assayed *in vitro* as inhibitors of fungal growth, we identified 8 (**1b**, **14**, **15**, **20**, **21**, **25**, **27** and **28**) with improved antifungal activity against *Cochliobolus lunatus* compared to the parent compound **1a** (Figure 2). We have tested these compounds also against the deletion mutant (Δ*bph*) of CYP53A15. Since the observed antifungal activity of compounds against wild type and mutant fungal strain (not shown) is not statistically significantly different (Two way ANOVA with Bonferroni post test; $p<0.05$), we presume these compounds bind to and/ or inhibit also other, yet unidentified, molecular targets in *C. lunatus*.

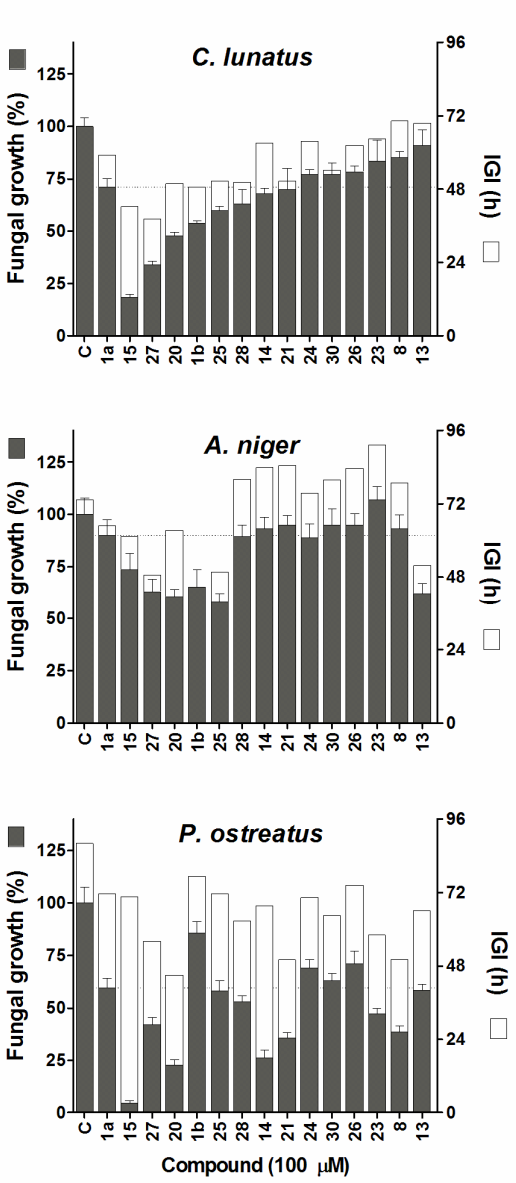

Figure 2. Antifungal activity of benzoic acid derivatives against *Cochliobolus lunatus*, *Aspergillus niger* and *Pleurotus ostreatus*. Fungal growth is expressed as a percentage of the matching control (C). Error bars indicate standard error from the mean (n = 3). Initial growth inhibition (IGI) is defined as an intercept on the time axis, whereby the linear growth phase is extrapolated to a zero increase in diameter.

We observed improved inhibition of *C. lunatus* fungal growth from the synthesized close analogue of **1a** (compound **1b**) compared to the parent compound, indicating steric hindrance when additional substituents, such as a methyl group (in **1a**), are present at the *meta* position of the **BA** phenyl ring. Substitution with two or more methyl groups (compounds **3**-**6**) significantly decreased the antifungal activity against all tested fungi. Similarly, in a study with *Aspergillus fumigatus* and *A. flavus* [35], moving the methyl, methoxy or chloro group on the **BA** phenyl ring in the direction *orto* > *meta* > *para* increased the antifungal activity of the tested compounds.

We also noticed that antifungal activity against *C. lunatus* is greatly influenced by *para* substitution on the phenyl ring. For example, the substitution of a pyrrole ring with less reactive thiophene increased the antifungal activity and produced the most

active compound (**15**) among all 37 derivatives of carboxylic acid. However, the thiophene-3-il derivative (**14**) exhibited almost 50% lower antifungal activity in comparison to the thiophene-2-il derivative (**15**). Similarly, the thiophene compounds extracted from the plant *Echinops ritro* (Astraceae) were reported previously as highly effective against fungal plant pathogens *Fusarium oxysporum*, *Phomopsis viticola*, *P. obscurans* and three different *Colletotrichum* species.[36]

Furthermore, we detected increased antifungal activity by the addition of fluoro or chloro substituents on the second phenyl ring (compounds **20**, **21**, and **25**) in comparison to the unsubstituted biphenyl derivative **24**. Fluoro derivatives were more active than chloro, and the *para* position was superior to the *meta* position on the second phenyl ring. Based on these findings, we synthesized a 2,4,5-trifluoro derivative (compound **27**) that confirmed our initial structure-antifungal activity information and showed the highest antifungal activity among biphenyl-4-carboxylic acid derivatives. The presence of three fluorines on the second phenyl ring significantly increased antifungal activity against *C. lunatus*, confirming that fluorine, in addition to increasing ligand metabolic stability and membrane permeation, can also enhance binding efficacy [37]. In contrast, 4-fluorobenzoic acid (compound **34**) had no antifungal properties, presumably due to the lack of a second ring system.

A non-aromatic 4-methylpiperidine derivative (compound **28**) also showed some antifungal properties; however, other derivatives with an aliphatic ring (pyrrolidine, piperidine, cyclohexyl) in the *para* position of **BA** (compounds **8**-**13**, **29**, **31**) lacked antifungal activity against *C. lunatus*. Most of the pyrrazole derivatives, purchased as close analogues of **1a**, were also inactive and we ascribed this to methylation of the pyrrazole ring (compounds **16**-**19**). When the carboxylic acid was replaced by sulphonic acid (compound **33**), the antifungal activity was lost. Interestingly, the presence of a polar acidic group on the second phenyl ring is not preferred and results in the loss of antifungal properties, as indicated by 4,4'-biphenyl-dicarboxylic acid (compound **35**). As expected, we detected no antifungal activity against *C. lunatus* for 1,4-benzenedicarboxylic acid (compound **36**) and naphthalene-2-carboxylic acid (compound **37**).

3.2.2. The antifungal activity of benzoic acid derivatives against Aspergillus niger.

The inhibition of *Aspergillus niger* growth (Figure 2) by selected benzoic acid derivatives produced a similar pattern of antifungal properties as observed for *C. lunatus* but resulted in six moderately active compounds. Compound **15** inhibited only 30% of fungal growth, compared to almost 80% inhibition of *C. lunatus* growth. Compounds **1b**, **20** and **25** showed similar antifungal properties in both fungi and in the same range as compound **15**. Compound **13** was equally effective, but selective towards *A. niger*. We noticed decreased antifungal activity of 2',4',5'-trifluoro-[1,1'-biphenyl]-4-carboxylic acid (compound **27**) against *A. niger*. Compounds with fluoro substituents on the second phenyl ring (**20**, **25** and **27**) again showed promising antifungal activity, while chloro substituents were less effective (compounds **21**-**23**). We detected no antifungal activity against *A. niger* for other benzoic acid derivatives (pyrrolidine, pyrrazole, piperidine, etc).

3.2.3. Pleurotus ostreatus growth inhibition.

We observed a different pattern of antifungal properties of benzoic acid derivatives against *P. ostreatus* (Figure 2). This was expected, since *P. ostreatus* belongs to the basidiomycetes, which have multiple CYP53 sequences in their genomes [20,21] and are speculated to have acquired other functions in addition to benzoate detoxification, such as involvement in the degradation of wood components.[14] It is possible that compounds interact with other two CYP53 predicted in the *P. ostreatus* genome and contribute in part to the observed antifungal effects. Nevertheless, compound **15** remained the most active benzoic acid derivative, almost completely inhibiting fungal growth at a 100 μM concentration. We also obtained promising results for compounds **14**, **20** and **21**, which exhibited around 75% inhibition of fungal growth. The presence of a thiophene ring (compound **14**) and fluoro substituted phenyl ring in the *para* position of **BA** (compound **20**) was again confirmed as the best selection for promising antifungal activity. Interestingly, compound **1b** showed lower antifungal activity than the parent compound **1a**, indicating that steric effects are less important in *P. ostreatus*.

3.3. CYP53 sequence and structure conservation

Cytochromes P450 are highly diverse proteins and sequence identities between distant CYP families may be less than 15%.[38] Using the T-Coffee alignment tool, we determined the amino acid sequence conservation of selected CYP53 members (Figure 3). Ascomycete CYP53A15 from *Cochliobolus lunatus* and CYP53A1 from *Aspergillus niger* belong to CYP53 subfamily A and share 66% sequence identity. Basidiomycete *Pleurotus ostreatus* CYP53C11 is a member of CYP53 subfamily C and has 54% and 50% amino acid residues identical to CYP53A15 and CYP53A1, respectively. Among 94 protein sequences in a protein alignment of the CYP53A subfamily (http://www.cyped.uni-stuttgart.de/CONTENT/aln/aln971.html) in the CYPED database [31], only 18 amino acid residues are identical, while 78 amino acid positions were conserved.

The available crystal structures of cytochromes P450 show a similar protein tertiary structure, which is predominantly composed of α-helices labeled A to L (starting from the N-terminus) and β-strands numbered 1-5; with the enzyme active site buried deep in the core of the protein next to the heme prosthetic group.[39–41] The spatial conservation of CYP structures is the highest in the regions associated with binding of heme and protein redox partners.[38,41] The characteristic P450 consensus sequence (CxG) with an absolutely conserved Cys residue (as fifth ligand to the heme iron) is located just before the L helix in the β-bulge region (called the Cys pocket).[33,38] The second conserved motif (ExxR in the K helix) is important for the stabilization of the meander loop and probably for the maintenance of the core structure.[33] The central part of the I helix (A/G-G-x-D/E-T-T/S) corresponds to the putative oxygen binding motif.[42] The reductase interaction sites are proposed in the helices J/J' and in the insertion between the meander loop and the Cys pocket.[39] The highest variability and flexibility are in the substrate recognition sites [43] (SRS 1-6; Figure 3) that are located in the termini of helices F and G, forming the "roof" of the active site cavity, and helix I on one side of the heme and helix K, β-strands 1-4 and 4-1 and the BC loop on the opposite side.[39,41]

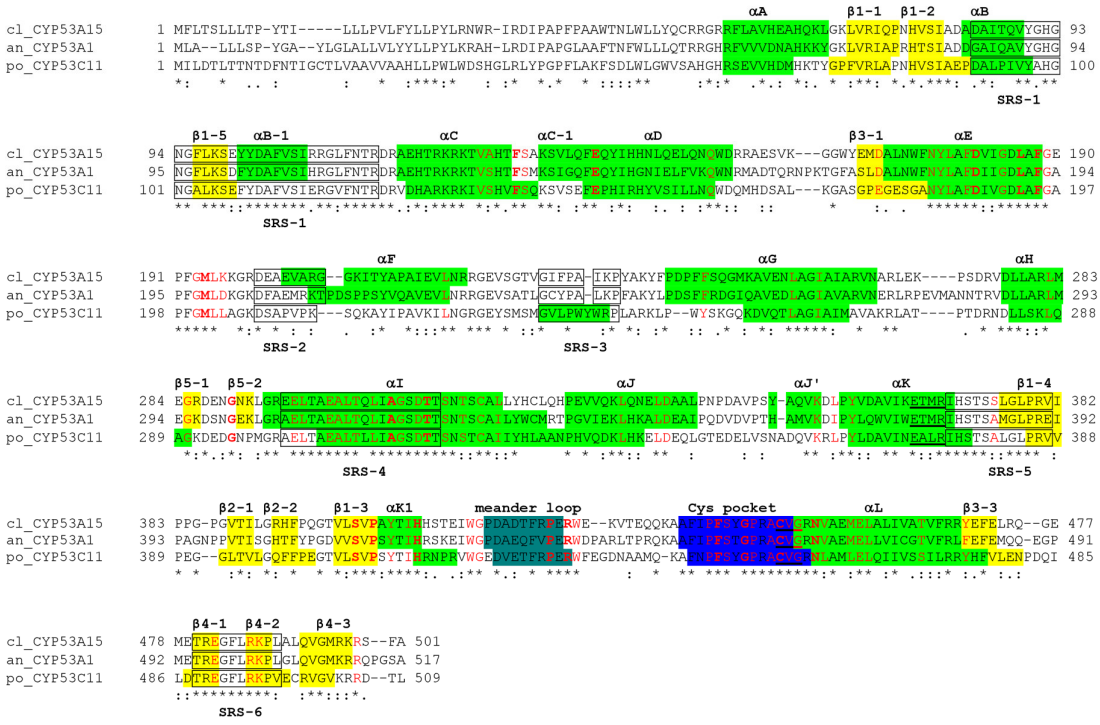

Figure 3. Amino acid sequence alignment of selected CYP53 enzymes indicating conserved secondary structure elements and variable substrate recognition sites (SRS; boxed). Red letters mark residues that are conserved and strictly conserved (bold) among 94 proteins of the CYP53A subfamily in the CYPED database.[31] Predicted secondary structure elements [39,32] are highlighted green (α-helices) and yellow (β-sheets). Underlined residues indicate cytochrome P450 signature motifs ExxR and CxG.[33] The Cys pocket region is highlighted blue and the meander loop is colored dark green.

3.4. CYP53 modeling

The enzymatic activity of CYP53 family members is mainly restricted to 4-hydroxylation of benzoate and some mono-substituted benzoate derivatives, indicating precision in substrate recognition and catalysis. Using the *Cochliobolus lunatus* CYP53A15 model [13] with inhibitor **1a** as a template [23], we constructed three CYP53 homology models labeled clCYP53A15, anCYP53A1 and poCYP53C11 (Figure 4) to provide an explanation of such precision, based on protein structural information. All models generated in this work were aligned to the crystal structure of *Saccharomyces cerevisiae* CYP51 [44] (PDB 4LXJ, data not shown), currently the only available fungal cytochrome P450 crystal structure. The overall RMSD parameter for backbone residues, which reflects the similarity between the compared structure and *Saccharomyces cerevisiae* CYP51, were calculated to be 3.0, 5.1, 7.7 Å for anCYP53A1, poCYP53C11 and clCYP53A15, respectively. We noticed that the amino acid residues involved in the binding of heme and stabilization of the CYP core structure are always placed in similar positions and this structural folding is energetically favorable. This trend has also been observed in the folding of over 6,000 artificial chimeric P450 heme proteins created by SCHEMA-guided recombination of parent cytochromes P450.[45]

Most eukaryotic cytochromes P450 are membrane bound proteins and presumably utilize various substrate access and product egress routes.[40,46] A hydrophobic substrate is likely to enter the buried active site from the membrane through the pw2a channel and the hydroxylated water-soluble product exits through pw2c. The pw2a channel opening is in the lipid membrane and lies between the FG loop and the B' helix/BC loop, while pw2c is located between the B' helix/BC loop and helices G and I.[40] We noticed that in the clCYP53A15 model, the channel with inhibitor **1a** traveling to the active site cavity above the heme plane is opened and easily accessible (Figure 4a). However, in the anCYP53A1 model, two regions confine access to the catalytically active heme iron (Figure 4b). The first region is part of SRS5 and consists of residues P-R-E-I-P-A (positions 389-394) in the β1-4 strand. Due to the flanking proline residues, the flexibility of this region is limited and restricts the passage of the inhibitor to the active site cavity. The second region, comprised of residues S-D-F-Y-D (positions 100-104) in the B-1 helix, is part of SRS1. It protrudes towards the heme, preventing the inhibitor from making a turn and approaching the heme at an appropriate angle. Access to the active site of the anCYP53A1 model is additionally sterically restricted by residue F-43 and the charge restricted by residue R-77, both residues in this way acting as a gating mechanism for substrate/inhibitor specificity. In the poCYP53C11 model (Figure 4c), passage of the inhibitor is restricted to a certain extent by S-E-F-Y-D (positions 106-110) in the SRS1 region. Unlike in anCYP53A1, this part is not rigid and allows a slight movement of the loop to accommodate the inhibitor. The second region, narrowing the inhibitor pathway towards the heme iron, resides in SRS6 and consists of residues R-E-G (positions 489-491) in the β4-1 strand. Although, the M-

233 residue in poCYP53C11 is incapable of sterically blocking inhibitor entrance, as F-43 and R-77 residues in anCYP53A1 do, this residue adds a charge restriction for inhibitor specificity.

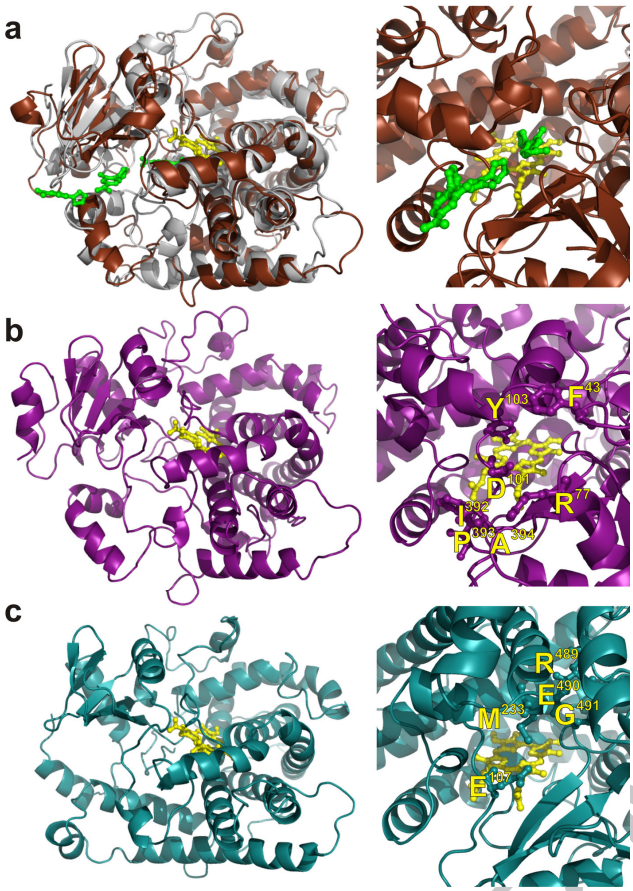

Figure 4. Comparison of CYP53 homology models from (**a**) *Cochliobolus lunatus* clCYP53A15 (brown) and the previously published model [23] (gray), (**b**) *Aspergillus niger* anCYP53A1 (violet) and (**c**) *Pleurotus ostreatus* poCYP53C11 (cyan). Inhibitor **1a** (green) and heme (yellow) are indicated in stick mode, while CYP53 enzymes are shown in a cartoon presentation. The residues narrowing the inhibitor pathway in anCYP53A1 and poCYP53C11 enzyme models are shown in violet and cyan sticks, respectively.

3.5. Docking reveals differences in the CYP53-ligand interactions

CYP53 enzymes are membrane-bound proteins and solving their crystal structure remains a challenging task. However, with homology modeling based on a previously published template [13], we generated energy minimized 3D models of selected CYP53 enzymes and performed HADDOCK solvated docking [47] of CYP53 substrate (**BA**), product (**4-HBA**) and 38 ligands with a potential antifungal activity. A total of 200 models was generated for each compound in the rigid body docking step. The top 100 structures were then subjected to refinement steps with a flexible interface and a water layer around the complex to obtain high quality predictions of complex structures in clusters sorted according to HADDOCK score (SI Table S1). HADDOCK docking scores for the CYP53A15 model ranged from −22.9 ± 6.7 for substrate (**BA**) to −63.2 ± 8.9 for compound **3**. We obtained similar results for the CYP53A1 model with substrate and compound **34**, which had the lowest scores of −16.9 ± 1.7 and −14.4 ± 2.6, respectively; while the highest score (−41.0 ± 2.7) was attributed to compound **33**. Docking the compounds into the CYP53C11 model resulted in HADDOCK scores ranging from −45.0 ± 0.7 for compound **34** to −82.6 ± 3.9 for compound **9**. The size of the interface in a protein-ligand complex is indicated by the buried surface area (BSA).[25] In the CYP53A15 model, the BSA ranges between 308.2 ± 16.3 Å^2 for **BA** and 545.8 ± 21.7 Å^2 for compound **27**. A similar range of BSA values, from 330.5 ± 8.0 Å^2 (**BA**) to 585.8 ± 25.7 Å^2 (**27**), was also calculated for the CYP53A1 model, while the ligand-CYP53C11 complex interface varied from 302.9 ± 10.0 Å^2 (**BA**) to 575.8 ± 24.7 Å^2 (**33**).

We grouped the compounds into 7 categories, based on the nature of the ring system at the *para* position of the BA phenyl ring, and compared the energy contributions (electrostatic, van der Waals and desolvation) for each ligand-CYP53 combination (Figure 5). The electrostatic interactions are the most significant contributor in the binding of compounds to all three CYP53 models indicated by large negative energy values. However, there are considerable differences among CYP53 enzymes. While CYP53C11 favors displacement of water molecules from the active site cavity on ligand binding, whereby water molecules possibly mediate H-bonds interactions between the enzyme and ligands, the desolvation of CYP53A1 and CYP53A15 is energetically unfavorable and water molecules possibly mediate charge-charge interactions between the enzyme and ligands. Furthermore, we noticed favorable van der Waals contributions (E value less than −10 kJ/mol), possibly stabilizing CYP53A1 and CYP53C11 interactions with the compounds, while these effects are less pronounced in CYP53A15-ligand interactions, with a few exceptions.

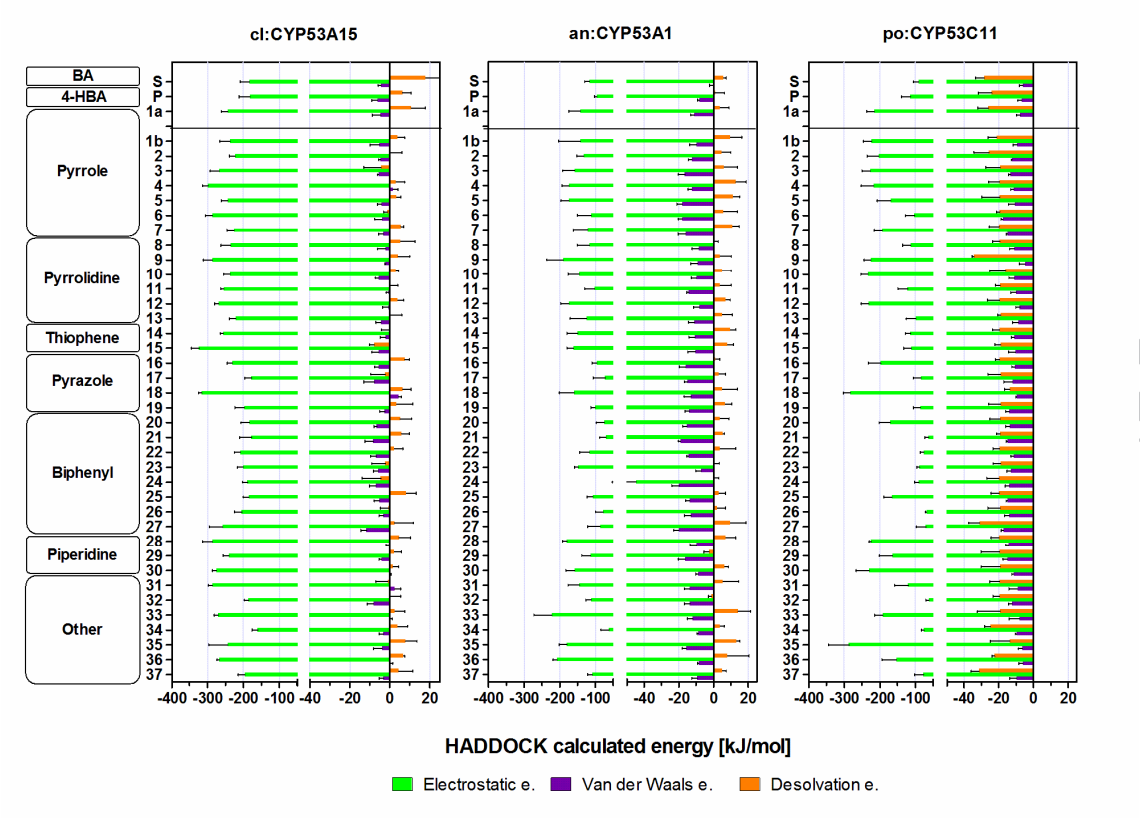

Figure 5. Van der Waals, electrostatic and desolvation energy as calculated by HADDOCK [47] for each CYP53 enzyme model and compound combination.

As with other cytochromes P450 [40,46], with the molecular docking of the most active compounds in the clCYP53A15 model and molecular dynamics simulation (Figure 6), we predicted various pathways leading to the CYP53A15 active site cavity above the heme plane. The substrate (**BA**) probably enters the pw2a channel lined by αF- and αI-helices and β1-4, β2-1, β4-1 and β4-2-sheets. The **BA** in the active site cavity is oriented perpendicular to the heme plane, sloped by 80°, with COOH group oriented away from the heme plane (Figure 6a). The query compound (**1a**) and compounds **15**, **27**, and **20** all access the CYP53A15 active site cavity via the pw2 channel formed by similar helices and strands as described above (Figure 6b-e). Their orientation towards the heme plane in the active site cavity is horizontal, sloped by 20°, with the COOH group pointing away from the heme. We observed that the most active compound (**15**) travels through the pw2a channel and then turns inside the active site cavity, finally to position itself with the carboxyl group towards the substrate access channel (Figure 6c; circled) thereby preventing the passage of the **BA** to the catalytic core. Docking of inactive compound **18** (Figure 6f) indicates that this compound only interacts with the residues at the CYP53A15 protein surface.

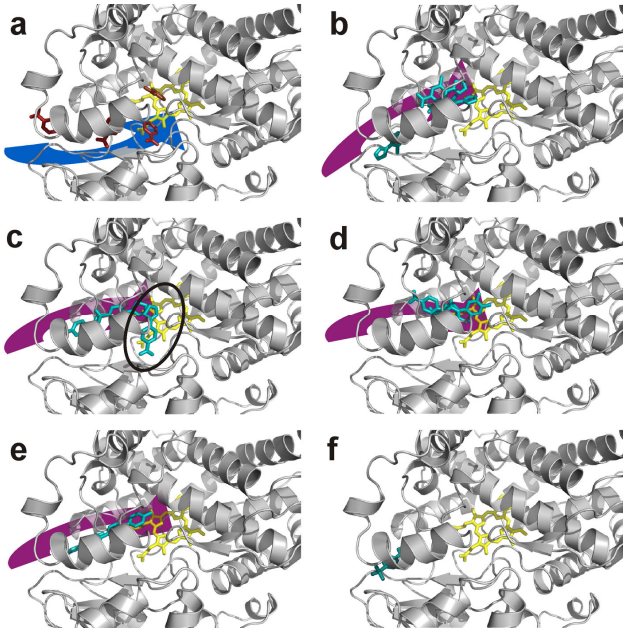

Figure 6. The most likely passage of substrate and putative inhibitors from the protein surface to the active site of clCYP53A15. The 3D HADDOCK models of inhibitor-clCYP53A15 enzyme complexes were superimposed on the clCYP53A15 enzyme alone using the Pymol 1.3 program (DeLano WL, http://www.pymol.org). The clCYP53A15 enzyme is shown in a gray cartoon presentation; inhibitors (cyan), substrate (brown), heme (yellow) are in stick presentation. **a**, benzoic acid; **b**, compound **1a**; **c**, compound **15**; **d**, compound **27**; **e**, compound **20**; **f**, compound **18**.

Using the CYP53A1 model and antifungal active compounds in the molecular docking and molecular dynamics simulation (Figure 7) provided an explanation for the lower activity. The substrate (**BA**) can enter the CYP53A1 active site cavity via 2 different channels. One is similar to the CYP53A15 pw2a channel, but at a 15° slope, lined by αF- and αI-helices and the β1-4-sheet, and the second is channel linked by αI-helix and β4-1 and β4-2-sheets. **BA** binding to both sites seems equally possible, since the energy of the models in both states is similar. The final position of **BA** above the heme plane is perpendicular, sloped by 60°, with the COOH group oriented away from the heme. The majority of compounds that moderately inhibit *A. niger* growth are bound at the rim of channel pw2a. The only compound that inserts into the active site cavity is compound **27**, which positions with the COOH group away from the heme and with rings oriented horizontally to the heme at a slope of 15°, by also blocking the second **BA** pathway. Although other compounds enter the pw2a channel, the reason for their inactivity or partial inactivity may be an inability to block the **BA** secondary channel path.

Molecular docking of active benzoic acid derivatives in the CYP53C11 model revealed that all compounds travel via the same access channel as **BA** but to different depths (Figure 8). The **BA** channel in this enzyme is similar to the pw2a anCYP53A1 channel and **BA** is oriented into the active cavity, similarly as in clCYP53A15. All compounds position with the COOH group away from the heme and with rings oriented horizontally to the heme at a slope of 15°.

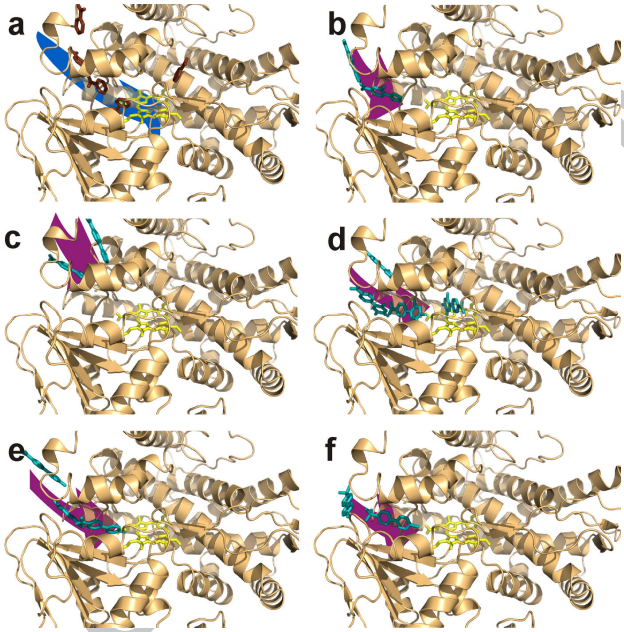

Figure 7. The most likely passage of substrate and putative inhibitors from the protein surface to the active site of anCYP53A1. The 3D HADDOCK models of inhibitor- anCYP53A1 enzyme complexes were superimposed on the anCYP53A1 enzyme alone using the Pymol program (DeLano WL, http://www.pymol.org). The anCYP53A1 enzyme is shown in a golden cartoon presentation; inhibitors (cyan), substrate (brown), heme (yellow) are in stick presentation. **a**, benzoic acid; **b**, compound **1a**; **c**, compound **15**; **d**, compound **27**; **e**, compound **20**; **f**, compound **33**.

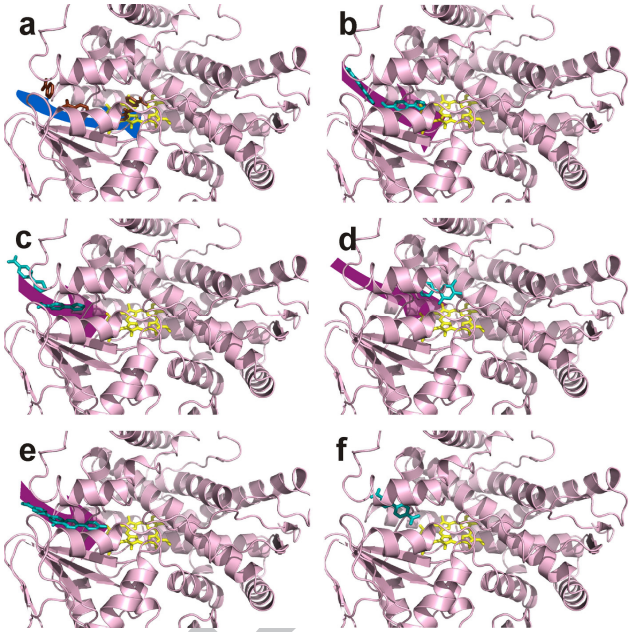

Figure 8. The most likely passage of substrate and putative inhibitors from the protein surface to the active site of poCYP53C11. The 3D HADDOCK models of inhibitor- poCYP53C11 enzyme complexes were superimposed on the poCYP53C11 enzyme alone using the Pymol program (DeLano WL, http://www.pymol.org). The poCYP53C11 enzyme is shown in a light purple cartoon presentation; inhibitors (cyan), substrate (brown), heme (yellow) are in stick presentation. **a**, benzoic acid; **b**, compound **1a**; **c**, compound **15**; **d**, compound **27**; **e**, compound **20**: **f**, compound **35**.

4. Conclusions

The antifungal activity of **BA** and its derivatives is well documented in yeasts and is based on the undissociated lipophilic acid form, which can permeate the plasma membrane and cause intracellular acidification, which leads to oxidative stress, protein aggregation, lipid peroxidation and inhibition of membrane trafficking.[48,49] In an adaptive response, yeasts counteract these effects by activating H^+-ATPases, changing the lipid composition of the plasma membrane, remodeling the cell wall structure and detoxification via multidrug resistance transporters (in particular Pdr12p).[49] However, in the filamentous ascomycetes and basidiomycetes, the **BA** is primarily detoxified by CYP53 enzymes.[13,16,18] The critical role of CYP53 in the primary fungal metabolism, together with the absence of homologues in higher eukaryotes and relatively conserved active site cavity, make CYP53 an attractive target in antifungal research.[14,23]

In this study, we generated three structural models of CYP53 enzymes and evaluated the antifungal activity of benzoic acid derivatives against *Cochliobolus lunatus*, *Aspergillus niger* and *Pleurotus ostreatus*. We found 8 compounds with improved antifungal activity compared to the parent compound **1a**. Moreover, we determined the key structural features giving the compounds' antifungal properties: *i)* the carboxylic group is important for biological activity, *ii)* the small group substitutions on the **BA** phenyl ring at positions *orto* and *meta* decrease activity due to steric hindrance, *iii)* substitution of the pyrrole ring with the less reactive thiophene or fluorinated phenyl ring is beneficial, while other substitutions abolish the antifungal activity.

In addition to these findings, in our molecular docking and molecular dynamics experiments we predicted a gating mechanism involving π-stacked interactions (present also in other CYPs; e.g., human CYP3A4 [50]), the amino acid residues

contributing to H-bonding and charge-charge interactions with CYP53. The ligand COOH group, important for biological activity, is always positioned away from the catalytically active heme iron. In *C. lunatus* CYP53A15 (Figure 9; a-c), we observed that residues R-110 and T-212 direct the most active antifungal compound (**15**) deep towards the heme plane, R-109 and E-224 then mediate the turning and positioning of the compound at such an angle that it blocks the pathway for **BA**. As in our previous study [23], we found a possible second access channel for **BA**. The occurrence of two access channels for **BA** is even more probable in CYP53A1 from *A. niger*, but to be a successful inhibitor of CYP53A1 the compound has to close both channels. As seen in Figure 9 (d-f), compound **15** cannot penetrate deep into the enzyme active site due to the specific gating mechanism comprised of a π-stacking interaction with F-210 and H-bonding with R-77. In *Pleurotus ostreatus* CYP53C11 (Figure 9; g-i), amino acid residues W-200, R-39 and R-83 mediate H-bonding interactions with compound **15,** while T-69 contributes to the π-stacking interaction.

We believe that these data contribute to a better understanding of CYP53-ligand interactions by identifying possible substrate/ inhibitor channels and assist in the design of more potent and selective inhibitors targeting CYP53, thereby facilitating antifungal drug research.

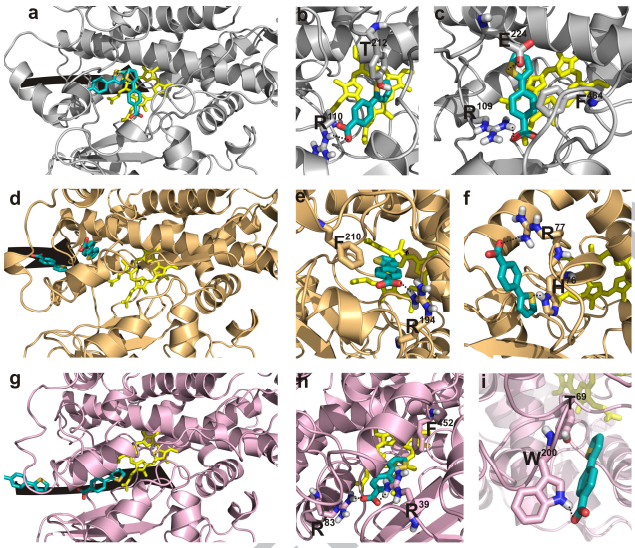

Figure 9. Compound **15** interactions with CYP53 enzyme models of *Cochliobolus lunatus* (**a-c**), *Aspergillus niger* (**d-f**) and *Pleurotus ostreatus* (**g-i**). The atomic coordinates of the HADDOCK models were superimposed on the model of clCYP53A15 using the Pymol program (DeLano WL, http://www.pymol.org). Inhibitor **15** (cyan) and heme (yellow) are in stick representation. Enzyme models are presented in cartoon representation.

Acknowledgments

We sincerely thank Dr. Samo Turk for the similarity-based virtual screening. We wish to acknowledge the help provided by Marko Bunc and Žan Koren in the synthesis and analysis of compounds as well as with antifungal screening. Thanks to David R. Nelson from Cytochrome P450 Nomenclature Committee for the naming of CYP53C11 from *Pleurotus ostreatus*. We thank Martin Cregeen for language editing. We thank OpenEye Scientific Software, Inc. for free academic licenses for their software. We are grateful for the financial support of the Slovenian Research Agency by Grants J4-2212, P1-0104 and P1-0207.

Supplementary Material

Supplementary data (Table S1, Chemical characterization, Model quality evaluation and ^{1}H and ^{13}C NMR spectra) associated with this article can be found, in the online version, at .

References and notes

1. In *Fungal Research Trust 20 th Anniversary meeting.*; London, **2011**.
2. Pennisi, E. *Science* **2010**, *327*, 804–5.
3. Fisher, M. C.; Henk, D. A.; Briggs, C. J.; Brownstein, J. S.; Madoff, L. C.; McCraw, S. L.; Gurr, S. J. *Nature* **2012**, *484*, 186–94.
4. Sheng, C.; Zhang, W. *Curr. Med. Chem.* **2011**, *18*, 733–66.
5. Ostrosky-Zeichner, L.; Casadevall, A.; Galgiani, J. N.; Odds, F. C.; Rex, J. H. *Nat. Rev. Drug Discov.* **2010**, *9*, 719–27.
6. Grigoriev, I. V; Nikitin, R.; Haridas, S.; Kuo, A.; Ohm, R.; Otillar, R.; Riley, R.; Salamov, A.; Zhao, X.; Korzeniewski, F.; Smirnova, T.; Nordberg, H.; Dubchak, I.; Shabalov, I. *Nucleic Acids Res.* **2014**, *42*, D699–704.
7. Cools, H. J.; Hammond-Kosack, K. E. *Mol. Plant Pathol.* **2013**, *14*, 197–210.
8. Liao, C.; Sitzmann, M.; Pugliese, A.; Nicklaus, M. C. *Future Med. Chem.* **2011**, *3*, 1057–85.
9. Gassner, N. C.; Tamble, C. M.; Bock, J. E.; Cotton, N.; White, K. N.; Tenney, K.; St Onge, R. P.; Proctor, M. J.; Giaever, G.; Nislow, C.; Davis, R. W.; Crews, P.; Holman, T. R.; Lokey, R. S. *J. Nat. Prod.* **2007**, *70*, 383–90.
10. Srinivasan, A.; Leung, K. P.; Lopez-Ribot, J. L.; Ramasubramanian, A. K. *MBio* **2013**, *4*.
11. Črešnar, B.; Petrič, S. *Biochim. Biophys. Acta* **2011**, *1814*, 29–35.
12. Kelly, S. L.; Kelly, D. E. *Philos. Trans. R. Soc. Lond. B. Biol. Sci.* **2013**, *368*, 20120476.
13. Podobnik, B.; Stojan, J.; Lah, L.; Kraševec, N.; Seliškar, M.; Rižner, T. L.; Rozman, D.; Komel, R. *J. Med. Chem.* **2008**, *51*, 3480–6.
14. Jawallapersand, P.; Mashele, S. S.; Kovačič, L.; Stojan, J.; Komel, R.; Pakala, S. B.; Kraševec, N.; Syed, K. *PLoS One* **2014**, *9*, e107209.
15. Fukuda, H.; Nakamura, K.; Sukita, E.; Ogawa, T.; Fujii, T. *J. Biochem.* **1996**, *119*, 314–8.
16. Faber, B. W.; van Gorcom, R. F.; Duine, J. A. *Arch. Biochem. Biophys.* **2001**, *394*, 245–54.
17. Fraser, J. A.; Davis, M. A.; Hynes, M. J. *Fungal Genet. Biol.* **2002**, *35*, 135–46.
18. Matsuzaki, F.; Wariishi, H. *Biochem. Biophys. Res. Commun.* **2005**, *334*, 1184–90.

19. Harwood, C. S.; Parales, R. E. *Annu. Rev. Microbiol.* **1996**, *50*, 553–90.

20. Ide, M.; Ichinose, H.; Wariishi, H. *Arch. Microbiol.* **2012**, *194*, 243–53.

21. Moktali, V.; Park, J.; Fedorova-Abrams, N. D.; Park, B.; Choi, J.; Lee, Y.-H.; Kang, S. *BMC Genomics* **2012**, *13*, 525.

22. Degani, O. *Adv. Biosci. Biotechnol.* **2014**, *05*, 340–352.

23. Berne, S.; Podobnik, B.; Zupanec, N.; Novak, M.; Kraševec, N.; Turk, S.; Korošec, B.; Lah, L.; Šuligoj, E.; Stojan, J.; Gobec, S.; Komel, R. *J. Chem. Inf. Model.* **2012**, *52*, 3053–63.

24. Korošec, B.; Sova, M.; Turk, S.; Kraševec, N.; Novak, M.; Lah, L.; Stojan, J.; Podobnik, B.; Berne, S.; Zupanec, N.; Bunc, M.; Gobec, S.; Komel, R. *J. Appl. Microbiol.* **2013**.

25. De Vries, S. J.; van Dijk, M.; Bonvin, A. M. J. J. *Nat. Protoc.* **2010**, *5*, 883–97.

26. Irwin, J. J.; Sterling, T.; Mysinger, M. M.; Bolstad, E. S.; Coleman, R. G. *J. Chem. Inf. Model.* **2012**, *52*, 1757–68.

27. Zhu, R.; Xing, L.; Wang, X.; Cheng, C.; Su, D.; Hu, Y. *Adv. Synth. Catal.* **2008**, *350*, 1253–1257.

28. Molander, G. A.; Ryu, D.; Hosseini-Sarvari, M.; Devulapally, R.; Seapy, D. G. *J. Org. Chem.* **2013**, *78*, 6648–56.

29. Sheng, R.; Xu, Y.; Hu, C.; Zhang, J.; Lin, X.; Li, J.; Yang, B.; He, Q.; Hu, Y. *Eur. J. Med. Chem.* **2009**, *44*, 7–17.

30. López-Malo, A.; Alzamora, S. M.; Argaiz, A. *Food Microbiol.* **1995**, *12*, 213–219.

31. Fischer, M.; Knoll, M.; Sirim, D.; Wagner, F.; Funke, S.; Pleiss, J. *Bioinformatics* **2007**, *23*, 2015–7.

32. Gricman, Ł.; Vogel, C.; Pleiss, J. *Proteins* **2014**, *82*, 491–504.

33. Syed, K.; Mashele, S. S. *PLoS One* **2014**, *9*, e95616.

34. Arnold, K.; Bordoli, L.; Kopp, J.; Schwede, T. *Bioinformatics* **2006**, *22*, 195–201.

35. Kim, J. H.; Campbell, B. C.; Mahoney, N.; Chan, K. L.; Molyneux, R. J.; Balajee, A. *Fungal Biol.* **2010**, *114*, 817–24.

36. Fokialakis, N.; Cantrell, C. L.; Duke, S. O.; Skaltsounis, A. L.; Wedge, D. E. *J. Agric. Food Chem.* **2006**, *54*, 1651–5.

37. Müller, K.; Faeh, C.; Diederich, F. *Science* **2007**, *317*, 1881–6.

38. Werck-Reichhart, D.; Feyereisen, R. *Genome Biol.* **2000**, *1*, REVIEWS3003.

39. Sirim, D.; Widmann, M.; Wagner, F.; Pleiss, J. *BMC Struct. Biol.* **2010**, *10*, 34.

40. Schleinkofer, K.; Sudarko; Winn, P. J.; Lüdemann, S. K.; Wade, R. C. *EMBO Rep.* **2005**, *6*, 584–9.

41. Kirchmair, J.; Williamson, M. J.; Tyzack, J. D.; Tan, L.; Bond, P. J.; Bender, A.; Glen, R. C. *J. Chem. Inf. Model.* **2012**, *52*, 617–48.

42. Poulos, T. L.; Madrona, Y. *Biotechnol. Appl. Biochem.* **2013**, *60*, 128–33.

43. Lepesheva, G. I.; Waterman, M. R. *Mol. Cell. Endocrinol.* **2004**, *215*, 165–70.

44. Monk, B. C.; Tomasiak, T. M.; Keniya, M. V; Huschmann, F. U.; Tyndall, J. D. A.; O'Connell, J. D.; Cannon, R. D.; McDonald, J. G.; Rodriguez, A.; Finer-Moore, J. S.; Stroud, R. M. *Proc. Natl. Acad. Sci. U. S. A.* **2014**, *111*, 3865–70.

45. Otey, C. R.; Landwehr, M.; Endelman, J. B.; Hiraga, K.; Bloom, J. D.; Arnold, F. H. *PLoS Biol.* **2006**, *4*, e112.

46. Wade, R. C.; Winn, P. J.; Schlichting, I.; Sudarko *J. Inorg. Biochem.* **2004**, *98*, 1175–82.

47. Van Dijk, A. D. J.; Bonvin, A. M. J. J. *Bioinformatics* **2006**, *22*, 2340–7.

48. Hazan, R.; Levine, A.; Abeliovich, H. *Appl. Environ. Microbiol.* **2004**, *70*, 4449–57.

49. Mira, N. P.; Teixeira, M. C.; Sá-Correia, I. *OMICS* **2010**, *14*, 525–40.

50. Fishelovitch, D.; Shaik, S.; Wolfson, H. J.; Nussinov, R. *J. Phys. Chem. B* **2009**, *113*, 13018–25.